Shock Waves (1994) 4:25–34

Shock Waves

Restoration of the contact surface in the HLL-Riemann solver

E.F. Toro, M. Spruce, W. Speares

Department of Aerospace Sciences, College of Aeronautics, Cranfield Institute of Technology, Cranfield, Beds. MK43 0AL, UK

Received February 21, 1993; accepted March 24, 1993

Abstract. The missing contact surface in the approximate Riemann solver of Harten, Lax, and van Leer is restored. This is achieved following the same principles as in the original solver. We also present new ways of obtaining wave-speed estimates. The resulting solver is as accurate and robust as the exact Riemann solver, but it is simpler and computationally more efficient than the latter, particulaly for non-ideal gases. The improved Riemann solver is implemented in the second-order WAF method and tested for one-dimensional problems with exact solutions and for a two-dimensional problem with experimental results.

Key words: Finite difference scheme, Numerical simulation, Riemann solver

1. Introduction

A powerful class of modern shock-capturing methods for computational fluid dynamics (CFD) are those based on solutions to local Riemann problems. These Riemann-problem based techniques are generally known as Godunov-type methods. They are high-order extensions of the first-order accurate method of Godunov (1959). Some of their attractive features are (a) ability to automatically capture clean, sharp, and correctly positioned discontinuities such as shock waves and contact surfaces (b) their accuracy throughout the flow field and (c) their intrinsic robustness. However, in comparison to traditional methods such as artificial viscosity methods for example, these techniques are regarded as being both complex and computationally expensive, at the root of which lies the solution of the Riemann problem. In a realistic computation this is solved billions of times. It is, therefore, justified to search for improved Riemann solvers that are simpler and computationally efficient, but obviously not at the cost of two fundamental features of Godunov-type methods, namely accuracy and robustness.

For ideal gases the gains in using efficient, approximate Riemann solvers are not very significant, as exact Riemann solvers have become very efficient (Toro 1989a). But for non-ideal gases exact Riemann solvers can be very expensive in comparison to approximate Riemann solvers. Our main motivation is the design of efficient and robust Godunov-type methods for real gases.

Several years ago Harten et al. (1983) presented an approach to solving the Riemann problem approximately. The resulting Riemann solvers have become known as HLL-Riemann solvers. The central idea was to assume a wave configuration for the solution consisting of two waves separating three constant states. This approach ignores the existence of intermediate waves. Also, it requires estimates for the speeds of the two assumed waves. For hyperbolic systems of two equations, such as the one-dimensional shallow water equations, the assumption of two waves only is correct but for larger systems, such as the Euler equations, it is not.

More recently Davis (1988) and Einfeldt (1988) have exploited these ideas in the context of the Euler equations by proposing wave-speed estimates and carrying out computations. The experience is that the resulting algorithms are indeed very efficient, robust and simple. Also, they handle sonic flow remarkably well. However their widespread use has been somewhat impeded by the highly undesirable feature of ruining contact surfaces. This results from having neglected the intermediate wave in the local Riemann problem. For certain applications, such as combustion problems, this defect can have undesirable consequences; contact surfaces carry discontinuities in temperature and internal energy and thus ignition criteria can fail due to poor numerical resolution of this kind of wave. For two and three-dimensional problems this anomaly will also result in unacceptable smearing of vortex sheets and shear waves.

In this paper we present an improved version of the HLL-Riemann solver by restoring the contact surface. This is achieved by applying the same principles as Harten et al. (1983). We call the modified Riemann solver, HLLC. We also present very efficient ways of finding wave-speed estimates. The resulting HLLC-Riemann solver is then implemented in the WAF method (Toro 1989b), a second-order TVD method of the Godunov type. Numerical results for

Correspondence to: E.F. Toro

one- and two-dimensional gas dynamics problems are presented for both ideal and covolume gases.

The rest of this paper is organized as follows. In Sect. 2 we recall the original HLL-Riemann solver. In Sect. 3 we discuss choices for the wave-speed estimates. In Sect. 4 we present the HLLC-Riemann solver with the restored contact surface. In Sect. 5 we implement HLLC in the WAF method. Section 6 contains test problems. Conclusions are drawn in Sect. 7.

2. The original HLL-Riemann solver

Here we recall the original HLL-Riemann solver in the context of the time-dependent, one-dimensional Euler equations.

2.1. The Euler equations

The Euler equations of gas dynamics in Cartesian coordinates, written in differential conservation-law form are

$$\mathbf{U}_t + [\mathbf{F}(\mathbf{U})]_x = 0. \tag{1}$$

$\mathbf{U}$ is the vector of conserved variables and $\mathbf{F}(\mathbf{U})$ is the vector of the corresponding fluxes, i.e.

$$\mathbf{U} = \begin{bmatrix} \rho \\ \rho u \\ E \end{bmatrix}, \quad \mathbf{F} = \begin{bmatrix} \rho u \\ \rho u^2 + p \\ u(E+p) \end{bmatrix}. \tag{2}$$

The conserved variables are: density ρ, momentum ρu, where u is the velocity, and total energy E, where $E = \rho u^2/2 + \rho e$ with e denoting specific internal, or intrinsic, energy.

The symbols t and x denote time and space and are the independent variables. The associated subscripts in (1) denote partial differentiation. Note that there are more dependent variables than equations and thus a closure condition is required; the equation of state $e = e(\rho, p)$ is taken to serve that role. In this paper we consider the ideal-gas equation of state and the covolume equation of state. These can be written as

$$e = e(\rho, p) = \frac{p(1 - b\rho)}{(\gamma - 1)\rho} \tag{3}$$

where γ is the ratio of specific heats and b is the covolume (constant). For $b = 0$ we recover the ideal gas equation of state.

The Euler equations have discontinuous solutions (shock waves, contacts) and it is therefore more appropriate to recast the differential equations (1) in integral form as

$$\oint (\mathbf{U}\mathrm{d}x - \mathbf{F}(\mathbf{U})\mathrm{d}t) = 0. \tag{4}$$

Conservative numerical methods are directly based on this integral form of the governing equations.

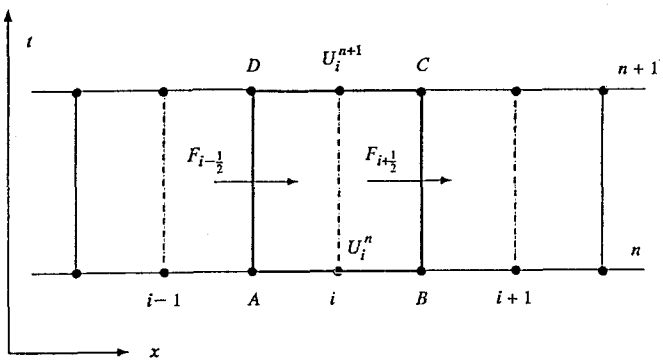

Fig. 1. Control volume of dimensions Δx by Δt is computational cell i. New value $\mathbf{U}_i^{n+1}$ is given in terms of old value $\mathbf{U}_i^n$ and intercell fluxes

2.2. Conservative numerical methods

Consider the grid configuration of Fig. 1 for a time-marching procedure. Evaluation of integral (4) in the control volume ABCD of dimensions Δx by Δt produces the scheme

$$\mathbf{U}_i^{n+1} = \mathbf{U}_i^n - \frac{\Delta t}{\Delta x}\left(\mathbf{F}_{i+\frac{1}{2}} - \mathbf{F}_{i-\frac{1}{2}}\right) \tag{5}$$

with suitable interpretations for the the discrete values of the conserved variables and fluxes. This explicit *conservative* formula gives a time-marching scheme in terms of the data $\mathbf{U}_i^n$, the grid dimensions Δx, Δt, and the intercell fluxes $\mathbf{F}_{i+1/2}$ and $\mathbf{F}_{i-1/2}$. The notation $\mathbf{U}_i^n$, means the discrete value of $\mathbf{U}$ in cell i at time level n. For convenience, we often omit the superscript n.

The scheme (5) is completely defined once the fluxes have been specified. Let us consider $\mathbf{F}_{i+1/2}$. Godunov-type methods utilise the solution of the local Riemann problem with data $(\mathbf{U}_i^n, \mathbf{U}_{i+1}^n)$ to define the numerical flux $\mathbf{F}_{i+1/2}$.

2.3. The Riemann problem

The Riemann problem for (1) is the initial value problem for (1) in the domain $-\infty < x < \infty$, $t > 0$ with initial data

$$\mathbf{U}(x, 0) = \begin{cases} \mathbf{U}_\mathrm{L}, & x < 0, \\ \mathbf{U}_\mathrm{R}, & x > 0. \end{cases} \tag{6}$$

The structure of the solution of the Riemann problem looks as depicted in Fig. 2. There are three waves. The middle wave is always a contact discontinuity. The left and right waves, which due to their character are called *non-linear waves*, can be either shocks or rarefactions and hence there are four possible wave patterns. Contacts and shocks are discontinuities, rarefaction waves are continuous solutions. The region between the non-linear waves has constant pressure p^* and constant velocity u^* and is called the *star* region. The density (and the internal energy) changes discontinuously across the contact surface from the constant value ρ_L^* to the left of the contact to the constant value ρ_R^* to the right of the contact. The complete solution is constant along rays emanating from the origin; it depends only on the similarity variable x/t and it is therefore denoted by $\tilde{\mathbf{U}}(x/t)$.

The first-order Godunov method (Godunov 1959) uses the solution $\tilde{\mathbf{U}}(x/t)$ of Riemann problem with data

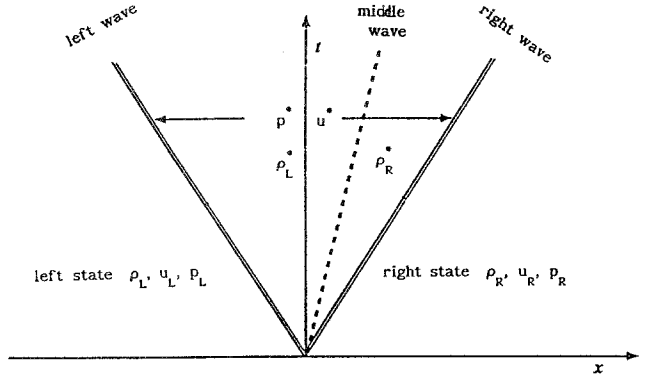

Fig. 2. Solution of the Riemann problem with data $\mathbf{U}_L$ and $\mathbf{U}_R$ in the x-t plane. The three waves present define four piece-wise constant states

$(\mathbf{U}_i^n, \mathbf{U}_{i+1}^n)$ along the t-axis $(x/t = 0)$ to define the intercell flux, that is $\mathbf{F}_{i+1/2}^{GOD} = \mathbf{F}[\tilde{\mathbf{U}}(0)]$.

2.4. The Harten-Lax-van Leer Riemann solver (HLL)

A very simple type of approximations to the solution of the Riemann problem was proposed by Harten et al. (1983). Their basic assumptions are: (a) the four possible wave patterns in the exact solution are represented by a single wave pattern, (b) the only waves present are the left and right non-linear waves and (c) *a-priori* estimates S_L and S_R for the lower and upper bounds of the speeds of these non-linear waves are available. As a consequence of (b) above there is no contact discontinuity and the whole of the star region is given by a constant vector $\mathbf{U}_{i+1/2}^*$. Under these assumptions one can easily solve for $\mathbf{U}_{i+1/2}^*$ and the corresponding flux vector $\mathbf{F}_{i+1/2}^*$ in the star region.

Consider Fig. 3 in which $S_L \leq 0$ and $S_R \geq 0$. Evaluation of the integral (4) in the rectangle ABCD gives directly

$$\mathbf{U}_{i+\frac{1}{2}}^* = \frac{S_R\mathbf{U}_R - S_L\mathbf{U}_L - (\mathbf{F}_R - \mathbf{F}_L)}{S_R - S_L} \tag{7}$$

where subcripts L and R replace i and $i+1$ and $\mathbf{F}_R = \mathbf{F}(\mathbf{U}_R)$, $\mathbf{F}_L = \mathbf{F}(\mathbf{U}_L)$. One can also compute a star flux directly as

$$\mathbf{F}_{i+\frac{1}{2}}^* = \frac{S_R\mathbf{F}_L - S_L\mathbf{F}_R + S_LS_R(\mathbf{U}_R - \mathbf{U}_L)}{S_R - S_L}. \tag{8}$$

This flux function form the basis for a Godunov-type method based on the conservative formula (5) with intercell numerical flux

$$\mathbf{F}_{i+\frac{1}{2}}^{HLL} = \begin{cases} \mathbf{F}_i, & S_L \geq 0, \\ \mathbf{F}_{i+\frac{1}{2}}^*, & S_L \leq 0 \leq S_R, \\ \mathbf{F}_{i+1}, & S_R \leq 0. \end{cases} \tag{9}$$

A major problem with this Riemann solver is to find reliable and sufficiently simple estimates S_L and S_R for the lower and upper bounds of the wave speeds, for which a great deal about the solution itself must be known in advance. Davis (1988) and Einfeldt (1988) proposed a number of procedures for these wave-speed estimates. A possible choice for S_L and S_R in (7)–(8) is the wave speeds given by the Roe

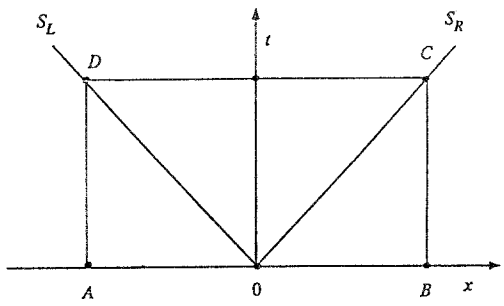

Fig. 3. Simplified wave structure for the original HLL approximate Riemann solver in case of subsonic flow

approximation (Roe 1981). Davis made the interesting observation that the choice $S_R = \Delta x/\Delta t$, $S_L = -S_R$ gives a flux $\mathbf{F}_{i+1/2}^*$ associated with the Lax-Friedrichs scheme. Other obvious choices reproduce star fluxes $\mathbf{F}_{i+1/2}^*$ associated with familiar schemes.

3. Wave speed estimates

Here we present three different ways of choosing estimates S_L and S_R for the wave speeds.

3.1. Isentropic estimates

Consider the isentropic equations of gas dynamics. This reduced hyperbolic system has two equations with eigenvalues $e_1 = u - a$ and $e_2 = u + a$, where a denotes the speed of sound. The solution of the associated Riemann problem has two waves; these are either shocks or rarefactions. Assume *a-priori* that these waves are rarefaction waves. Then we can find the exact solution for the speed u^* and the sound speed a^* between the non-linear waves, to this approximate problem. They are

$$\begin{aligned} u^* &= \frac{1}{2}(u_L - u_R) + \frac{a_L - a_R}{\gamma - 1}, \\ a^* &= \frac{1}{2}(a_L + a_R) + \frac{1}{4}(\gamma - 1)(u_L - u_R). \end{aligned} \tag{10}$$

Then we choose

$$\begin{aligned} S_L &= \min\{u_L - a_L, u^* - a^*\}, \\ S_R &= \max\{u_R + a_R, u^* + a^*\}. \end{aligned} \tag{11}$$

Note that there are two approximations here. First the Euler equations are approximated by the isentropic equations; then we assume that the two waves present in the solution of the Riemann problem for the reduced problem are rarefaction waves.

3.2. Linearized estimates

A local linearization of the Euler equations in primitive variables (Toro 1991) leads to the following approximation to the solution of the Riemann problem

$$
\begin{aligned}
p^* &= \frac{1}{2}(p_L + p_R) - \frac{1}{2}(u_R - u_L)\bar{\rho}\bar{a}, \\
u^* &= \frac{1}{2}(u_L + u_R) - \frac{1}{2}\frac{p_R - p_L}{\bar{\rho}\bar{a}}, \\
\rho_L^* &= \rho_L + \frac{(u_L - u_*)\bar{\rho}}{\bar{a}}, \\
\rho_R^* &= \rho_R + \frac{(u_* - u_R)\bar{\rho}}{\bar{a}}, \\
\bar{a} &= \frac{1}{2}(a_L + a_R), \\
\bar{\rho} &= \frac{1}{2}(\rho_L + \rho_R).
\end{aligned}
\tag{12}
$$

Then we define

$$
a_L^* = \sqrt{\frac{\gamma p^*}{\rho_L^*}}, \quad a_R^* = \sqrt{\frac{\gamma p^*}{\rho_R^*}} \tag{13}
$$

and choose wave speed estimates as

$$
\begin{aligned}
S_L &= \min\{u_L - a_L, u^* - a_L^*\}, \\
S_R &= \max\{u_R + a_R, u^* + a_R^*\}.
\end{aligned}
\tag{14}
$$

3.3. Hybrid estimates

Another possible way of selecting estimates is by using the exact wave-speed relations from the exact Riemann solver in conjunction with estimates for pressure p^* and particle speed u^*. In fact one can also obtain an estimate for the middle wave S_M of the contact surface, which is part of our improved version of the HLL solver to be described in Sect. 4. The wave speeds are given by

$$
S_L = u_L - a_L q_L, \quad S_M = u^*, \quad S_R = u_R + a_R q_R \tag{15}
$$

where the parameter q_S ($S = L$ and $S = R$) depends on the pressure ratio $H_S = p^*/p_S$ and is given by

$$
q_S = \begin{cases} 1, & H_S \le 1, \\ \sqrt{1 + \dfrac{\gamma+1}{2\gamma}(H_S - 1)}, & \text{otherwise.} \end{cases} \tag{16}
$$

It is now sufficient to find estimates for the pressure p^* and the particle speed u^*. This is a simpler task than finding wave speed estimates and several reliable choices are available. It is also worth noting that this procedure distinguishes between rarefactions and shocks. We have tested choice (15)–(16) with p^* and u^* as given by the linearized values in (12) and found it to be very satisfactory. The choice of p^* is more critical than that of u^*; it is this which determines the largest and smallest velocities and thus the CFL stability condition for numerical methods based on (5). It would be desirable to select a value of p^* greater than the true p_{ex}^* of the exact solution. This would result in speeds (15) for the shock case being larger than their counterpart in the exact solution. As for u^* we can use the approximate solution given in (12).

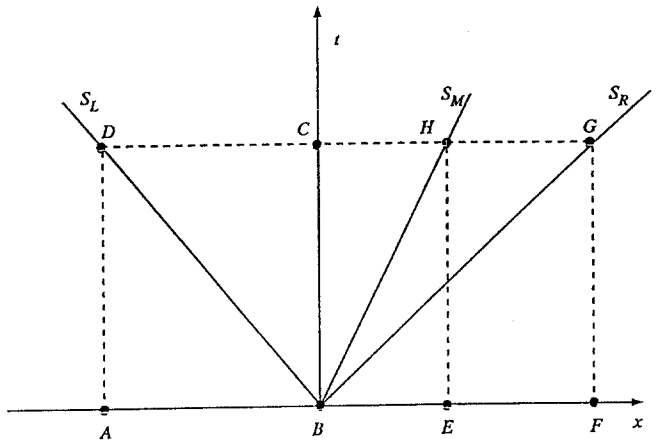

Fig. 4. Wave structure for the present HLLC-Riemann solver in case of subsonic flow

An alternative choice for the pressure is

$$
P_{TR}^* = \left\{ \left[\sum_{S=L,R} (1 - b\rho_S)a_S + \frac{(u_L - u_R)(\gamma - 1)}{2} \right] \Big/ \sum_{S=L,R} \frac{(1 - b\rho_S)a_S}{P_S^m} \right\}^{\frac{1}{m}}, \quad m = \frac{\gamma - 1}{2\gamma}. \tag{17}
$$

This expression is obtained from the assumption that both non-linear waves in the exact solution to the Riemann problem are rarefaction waves (Toro 1989a); it is valid for ideal as well as covolume gases. A corresponding value for u_{TR}^* can also be obtained directly. Our experience suggests that $p_{TR}^* \ge p_{ex}^*$, a conjecture that would be useful to prove.

3.4. Improved wave-speed estimates

Numerical tests, to be reported in Sect. 5, indicate that the isentropic and linearized choices are not sufficiently robust for very severe flow regimes, while the hybrid estimates are found to be both accurate and very robust. A way of incorporating robustness to the first two choices is as follows: from the estimates for S_L and S_R we compute $\mathbf{U}_{i+1/2}^* = [\rho^*, \rho^* u^*, E^*]^T$ as in (7). From here we obtain revised values for ρ^*, u^*, and p^* and thus revised values for $a^* = \sqrt{\gamma p^*/\rho^*}$. The new wave-speed estimates are then computed as in (11). This revised procedure is found to give very robust estimates S_L, S_M, and S_R.

4. The HLLC-Riemann solver

In this section we present the improved version HLLC of the Harten-Lax-van Leer Riemann solver by incorporating the contact surface into the wave pattern. We assume wave-speed estimates S_L, S_M, and S_R are available. These can be taken from the work of Sect. 3.

There are three wave patterns to consider, namely subsonic flow ($S_L \le 0$, $S_R \ge 0$); right supersonic flow ($S_L \ge 0$) and left supersonic flow ($S_R \le 0$). For subsonic flow con-

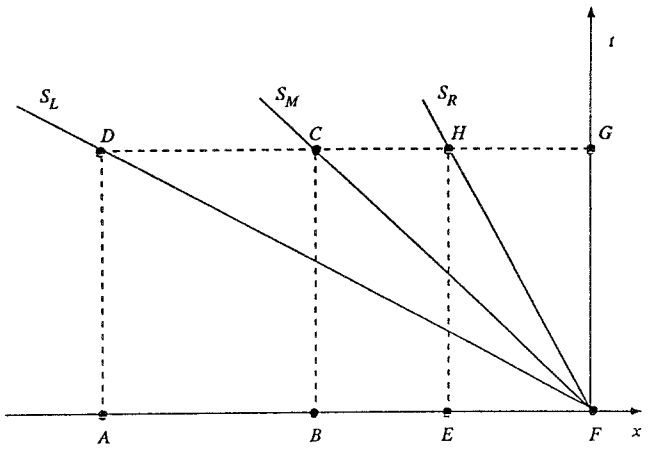

Fig. 5. Wave structure for the present HLLC-Riemann solver in case of left supersonic flow

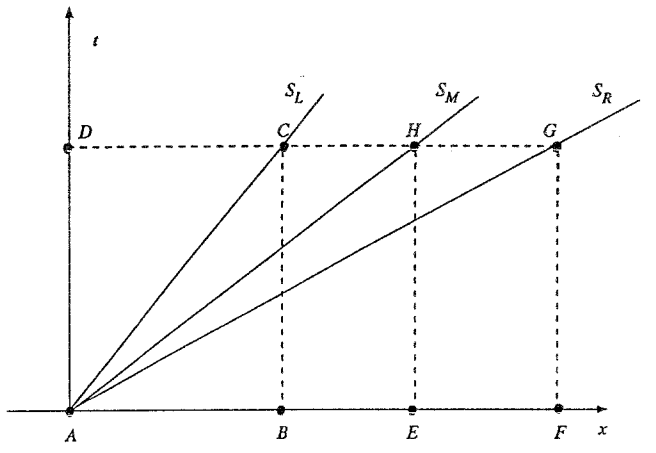

Fig. 6. Wave structure for the present HLLC-Riemann solver in case of right supersonic flow

sider the wave configuration of Fig. 4. Evaluation of the integral (4) in the quadrilateral ABCD gives

$$\mathbf{F}_L^* = \mathbf{F}_L + S_L(\mathbf{U}_L^* - \mathbf{U}_L). \tag{18}$$

Similarly, evaluation of (4) in the rectangle EFGH gives

$$\mathbf{F}_R^* = \mathbf{F}_R + S_R(\mathbf{U}_R^* - \mathbf{U}_R). \tag{19}$$

It is now a question of finding values for the vectors $\mathbf{U}_L^*$ and $\mathbf{U}_R^*$ in the right-hand sides of (18) and (19). Equation (18) can be expressed as

$$S_L\mathbf{U}_L^* - \mathbf{F}_L^* = S_L\mathbf{U}_L - \mathbf{F}_L = \mathbf{Q} \tag{20}$$

or in full as

$$S_L \begin{bmatrix} \rho_L^* \\ \rho_L^* u^* \\ E_L^* \end{bmatrix} - \begin{bmatrix} \rho_L^* u^* \\ \rho_L^* u^{*2} + p^* \\ u^*(E_L^* + p^*) \end{bmatrix} = \begin{bmatrix} q_1 \\ q_2 \\ q_3 \end{bmatrix}. \tag{21}$$

Note that the right hand-side $\mathbf{Q} = S_L\mathbf{U}_L - \mathbf{F}_L$ of (21) is known. Also note that the speed of the contact discontinuity is $u^* = S_M$. The first of equations (21) gives

$$\rho_L^* = \frac{q_1}{S_L - S_M}. \tag{22}$$

After some manipulations the second equation gives

$$p_L^* = S_M q_1 - q_2 \tag{23}$$

while the third equation gives

$$E_L^* = \frac{q_3 + S_M p_L^*}{S_L - S_M}. \tag{24}$$

From equations (22)–(24) the vector $\mathbf{U}_L^* = [\rho_L^*,\ \rho_L^* u^*,\ E_L^*]^T$ of conserved variables in the star region to the left of the contact discontinuity follows. Substitution into equation (18) gives the solution for the flux $\mathbf{F}_L^*$. The complete solution for the flux $\mathbf{F}_R^*$ in (19) is obtained in a similar manner. Equations (19) can be rearranged as

$$S_R\mathbf{U}_R^* - \mathbf{F}_R^* = S_R\mathbf{U}_R - \mathbf{F}_R = \mathbf{R}. \tag{25}$$

From these we obtain

$$\rho_R^* = \frac{r_1}{S_R - S_M}, \tag{26}$$

$$p_R^* = S_M r_1 - r_2, \tag{27}$$

$$E_R^* = \frac{r_3 + S_M p_R^*}{S_R - S_M} \tag{28}$$

and the vector $\mathbf{U}_R^* = [\rho_R^*, \rho_R^* u^*, E_R^*]$ in (19) is now determined and so the numerical flux $\mathbf{F}_R^*$ follows.

As the pressure in the star region is constant, in the exact solution, it seems appropriate to enforce this in (24) and (28) for the energies by taking the mean value of p_L^* and p_R^*. Numerical experiments suggest that such condition might not be necessary. One could also use the assumed estimate for p^* to compute E_L^* and E_R^* in (24) and (28) more directly.

The case in which the particle speed u^* is negative gives identical results as those obtained above for $u^* \geq 0$. There are two more cases to consider.

The wave pattern of Fig. 5 in which $S_L \leq S_M \leq S_R \leq 0$ is that of left supersonic flow. Evaluation of the integral (4) over the rectangle ABCD gives $\mathbf{F}_L^*$ as in the subsonic case, (18). To obtain $\mathbf{F}_R^*$ we evaluate (4) over the rectangle EFGH. The result is

$$\mathbf{F}_R^* = \left[S_M S_R(\mathbf{U}_R - \mathbf{U}_L) + \frac{S_M S_R \mathbf{F}_L}{S_L} - S_M\mathbf{F}_R + S_R\left(1 - \frac{S_M}{S_L}\right)\mathbf{F}_L^* \right] \Big/ (S_R - S_M). \tag{29}$$

For right supersonic flow assume the wave structure depicted in Fig. 6 for $0 \leq S_L \leq S_M \leq S_R$. Evaluation of (4) over the rectangle ABCD gives $\mathbf{F}_R^*$ as in the subsonic case, (19). The flux $\mathbf{F}_L^*$ is obtained by integrating (4) over the rectangle EFGH. The result is

$$\mathbf{F}_L^* = \left[S_L S_M(\mathbf{U}_R - \mathbf{U}_L) - \frac{S_L S_M \mathbf{F}_R}{S_R} + S_M\mathbf{F}_L - S_L\left(1 - \frac{S_M}{S_R}\right)\mathbf{F}_R^* \right] \Big/ (S_M - S_L). \tag{30}$$

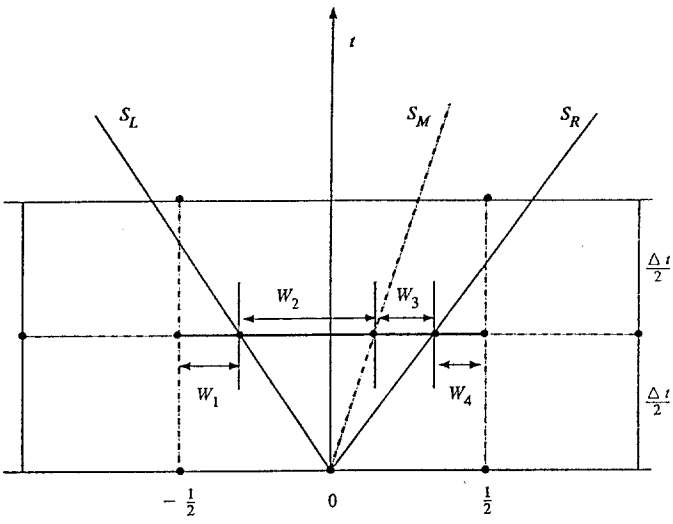

Fig. 7. Evaluation of the WAF numerical flux through the complete wave structure of the solution of the Riemann problem

5. Implementation in Godunov-type methods

The improved HLLC-Riemann solver can now be implemented in a whole range of Godunov-type methods. In this paper we consider the weigthed average flux method (Toro 1989b), or WAF.

5.1. The WAF method

The WAF method (Toro 1989b) is a second-order extension of Godunov's method. Higher accuracy is achieved by simply defining the intercell flux $\mathbf{F}_{i+1/2}$ as an integral average of the flux function $\mathbf{F}(\mathbf{U})$ in (1) evaluated at the solution $\tilde{\mathbf{U}}(x/t)$ of the Riemann problem with data $\mathbf{U}_i$, $\mathbf{U}_{i+1}$ at time $t = \Delta t/2$. An updated version of the method is found (Toro 1992a; 1992b). The WAF intercell numerical flux $\mathbf{F}_{i+1/2}$ is defined as

$$\mathbf{F}_{i+\frac{1}{2}} = \frac{1}{\Delta x} \int_{-\frac{\Delta x}{2}}^{\frac{\Delta x}{2}} \mathbf{F}\left(\tilde{\mathbf{U}}\left(\frac{x}{2\Delta t}\right)\right) \mathrm{d}x. \tag{31}$$

The integration can be made as accurate as desired, but the simple approximation

$$\mathbf{F}_{i+\frac{1}{2}} = \sum_{k=1}^{N+1} W_k \mathbf{F}_{i+\frac{1}{2}}^{(k)} \tag{32}$$

is found to be sufficiently accurate. The coefficients W_k (or weights) are the geometric extents of the constant states in the integral (31). $\mathbf{F}_{i+1/2}^{(k)}$ is the flux function $\mathbf{F}$ in (1) evaluated at the solution of the Riemann problem in region k. Figure 7 illustrates the situation. In the presence of sonic flow the *star* state closest to the t-axis is replaced by the solution along the t-axis, when using exact Riemann solvers. When using the HLLC-Riemann solver no special measures to deal with sonic flow are required.

It is easy to see that the weights W_k can be written in terms of the Courant numbers $\nu_k = \Delta t S_k/\Delta x$, with S_k the speed of wave k, as follows

$$W_k = \frac{1}{2}(\nu_k - \nu_{k-1}); \ \nu_0 = -1 \text{ and } \nu_{N+1} = +1. \tag{33}$$

Expression (32) can also be written, after using (33), as

$$\mathbf{F}_{i+\frac{1}{2}}^{\mathrm{WAF}} = \frac{1}{2}(\mathbf{F}_i + \mathbf{F}_{i+1}) - \frac{1}{2}\sum_{k=1}^{N} A_k \Delta\mathbf{F}_{i+\frac{1}{2}}^{(k)} \tag{34}$$

where

$$\Delta\mathbf{F}_{i+\frac{1}{2}}^{(k)} = \mathbf{F}_{i+\frac{1}{2}}^{(k+1)} - \mathbf{F}_{i+\frac{1}{2}}^{(k)} \tag{35}$$

is the flux jump across wave k. The coefficient A_k in (34) is a numerical viscosity function constructed on TVD (total variation diminishing) arguments to produce oscillation-free computed solutions. It can be constructed directly or through flux limiters B_k via the relation

$$A_k = 1 + \left(|\nu_k| - 1\right) B_k. \tag{36}$$

See Toro (1992a; 1992b) for details.

6. Test problems

In order to illustrate the performance of the improved HLLC-Riemann solver we present numerical results for one- and two-dimensional test problems.

6.1. Sod's shock tube problem

This test consists of solving the one-dimensional Euler equations (1) with ideal equation of state (3), $b = 0$, in a spacial domain of unit length and initial data

$$\rho_{\mathrm{left}} = 1.0, \ u_{\mathrm{left}} = 0, \ p_{\mathrm{left}} = 1.0,$$
$$\rho_{\mathrm{right}} = 0.125, \ u_{\mathrm{right}} = 0, \ p_{\mathrm{right}} = 0.1.$$

Here we take $\gamma = 1.4$; the left and right states are separated by a diaphragm positioned in the middle of the tube. The domain is discretised with 100 computing cells and the Courant number of the computations is 0.8.

Figure 8 shows a comparison between the computed solution, shown in symbols, and the exact solution, shown by full lines. The output time 0.25 units and the quantities shown are density, velocity, pressure, and specific internal energy. The internal energy is the most useful variable for assessing computed results. The Riemann solver used is the original HLL solver with wave speed estimates as in Sect. 3.3 and the numerical viscosity function A_k in (36) is the one corresponding to the flux limiter Superbee.

Figure 9 shows the corresponding result using our improved HLLC-Riemann solver. Note the dramatic improvement in the resolution of the contact discontinuity from about 20 points in the original HLL-Riemann solver to about 4 in the present HLLC version.

Figure 10 shows results for a sonic version of Sod's test problem, in which $u_{\mathrm{left}} = 3/4$. The initial discontinuity is at

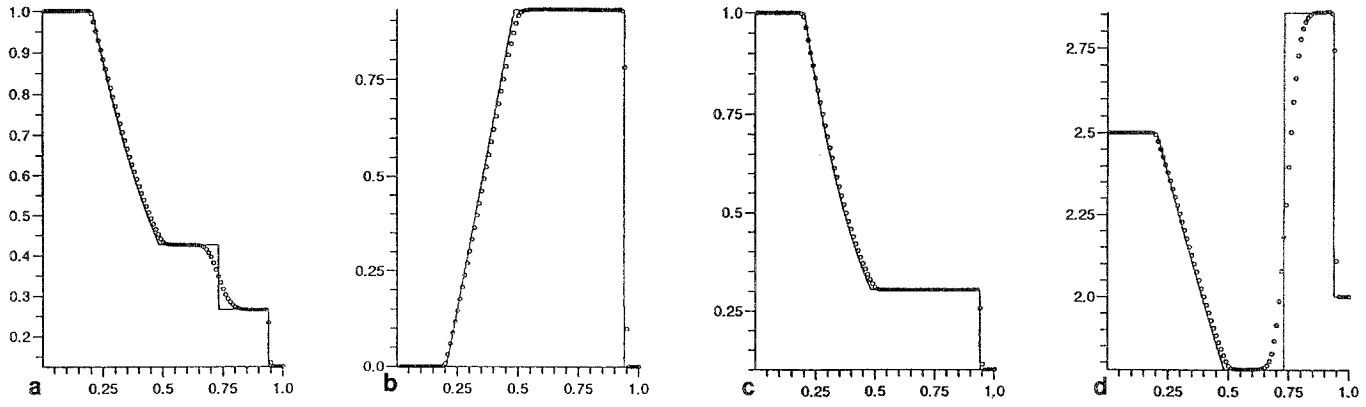

Fig. 8a–d. Comparison between the numerical (symbol) and exact (line) solutions for Sod's problem at time 0.25 units: **a** density; **b** velocity; **c** pressure; **d** specific internal energy. Numerical method used is WAF with the original HLL-Riemann solver

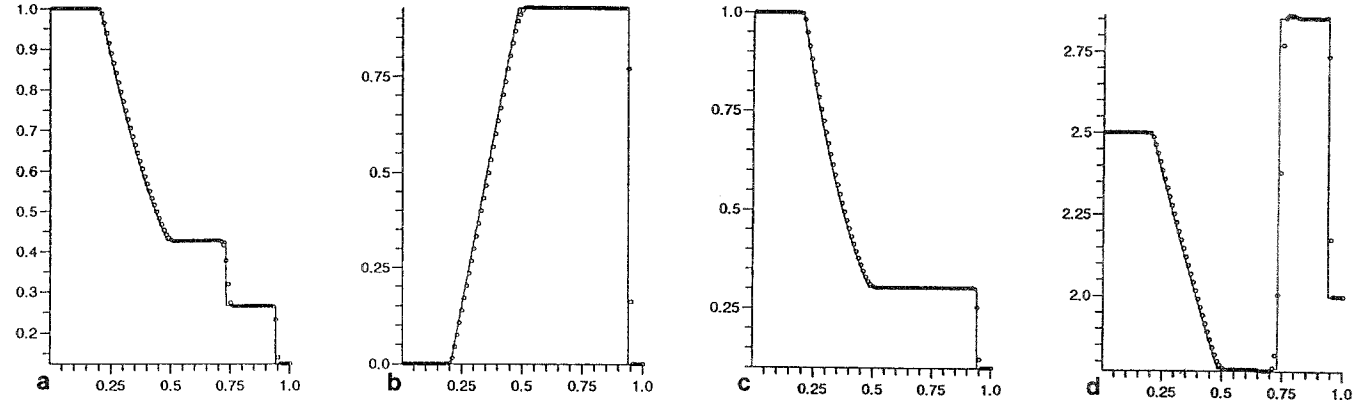

Fig. 9a–d. Comparison between the numerical (symbol) and exact (line) solutions for Sod's problem at time 0.25 units: **a** density; **b** velocity; **c** pressure; **d** specific internal energy. Numerical method used is WAF with the present HLLC-Riemann solver

$x = 0.4$. This test contains a sonic point and is used here to illustrate the fact that HLLC retains the good property of HLLC in dealing with sonic points. We use 100 cells.

6.2. The test of Woodward and Colella

This blast-wave problem to test the robustness of numerical methods was suggested by Woodward and Colella (1984). We solve the ideal, one-dimensional Euler equations with $\gamma = 1.4$ in a domain of unit length simulating a shock tube with two diaphragms placed at $x = 0.1$ and $x = 0.9$. The initial data consists of three constant states given by:

$$\rho_{\text{left}} = 1,\ u_{\text{left}} = 0,\ p_{\text{left}} = 1000.0,$$
$$\rho_{\text{middle}} = 1,\ u_{\text{middle}} = 0,\ p_{\text{middle}} = 0.01,$$
$$\rho_{\text{right}} = 1,\ u_{\text{right}} = 0,\ p_{\text{right}} = 100.0.$$

Figure 11 shows computed results at time 0.028 units in a grid of 3000 computing cells. This is a comparison between the numerical solution obtained when using the exact Riemann solver (line) and the present HLLC-Riemann solver. To plotting accuracy there is no difference in the results. Note the resolution of the contact discontinuities, especially in the specific internal energy.

Figure 12 shows a comparison between the original HLL (symbol) and the present HLLC (line) Riemann solvers. This corresponds to the results of Fig. 11. Note the resolution of the contacts; in the case of the strongest contact in the internal energy theHLL solver spreads the contact to about 450 points, while the HLLC solver does it in less than 10 points, as confirmed by Fig. 10.

Figure 13 shows a comparison between the performance of HLL and HLLC at time 0.038 on a grid of 500 cells. Note the obvious superiority of HLLC over the original HLL solver.

6.3. A shock tube problem with covolume

This test, first suggested by Einfeldt (1988), is like Sod's problem but for covolume gases with covolume $b = 0.8$ in the equation of state (3). Figure 14 shows a comparison between the numerical (symbol) and exact (line) solutions. For details on the exact solution for covolume gases see Toro (1989a). Again, the resolution of the contact discontinuity is very satisfactory.

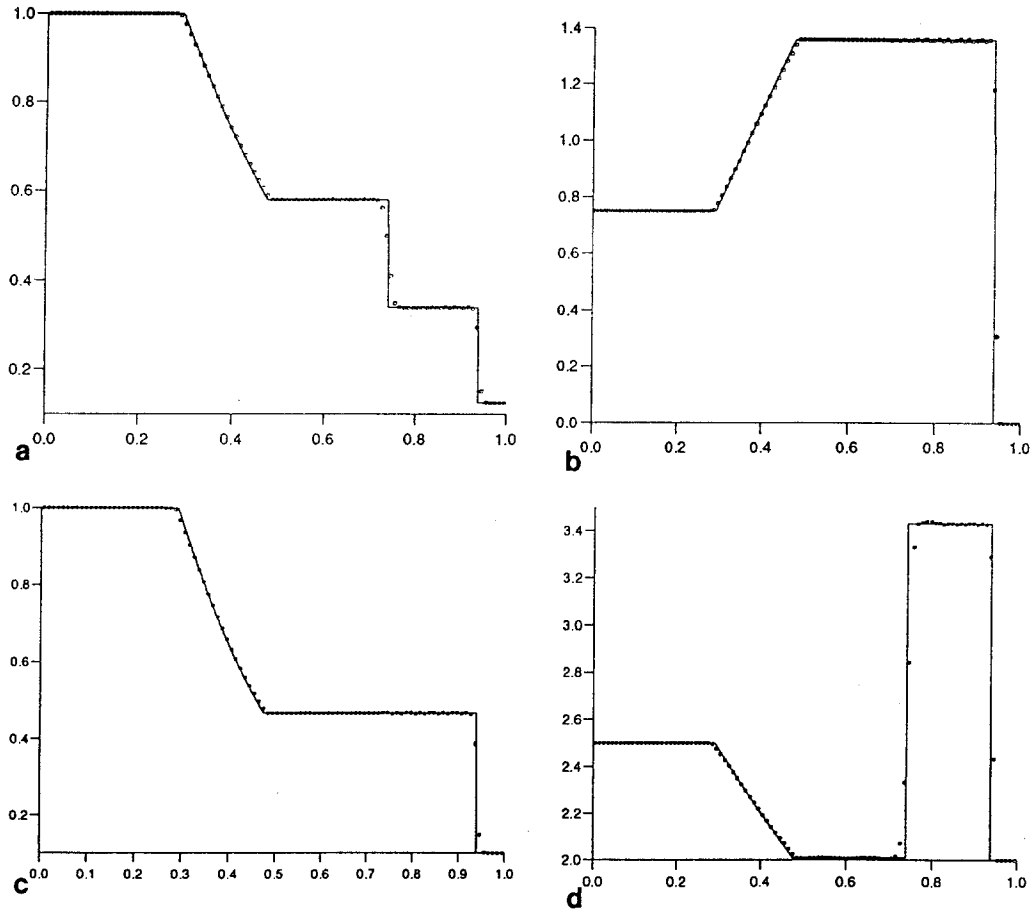

Fig. 10a–d. Comparison between the numerical (symbol) and exact (line) solutions for the sonic version of Sod's problem at time 0.25 units: **a** density; **b** velocity; **c** pressure; **d** specific internal energy. Numerical method used is WAF with the present HLLC-Riemann solver

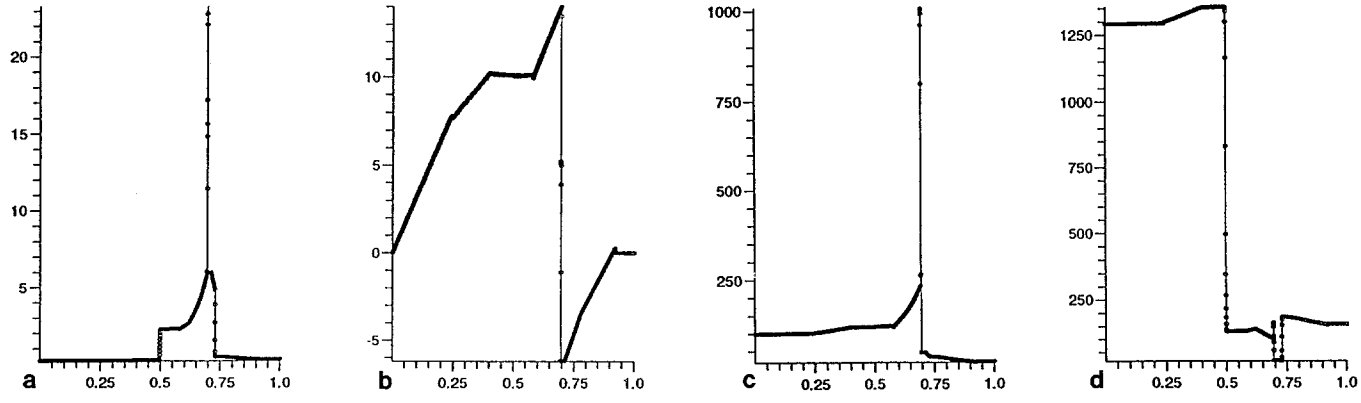

Fig. 11a–d. Comparison of performance between the present HLLC (symbol) and the exact (line) Riemann solvers used in the WAF method for the Woodward and Colella test problem at time 0.028 units: **a** density; **b** velocity; **c** pressure; **d** specific internal energy

6.4. Mach reflection

A problem of considerable interest is that of Mach reflection. Here we consider the reflection of an incident shock wave of Mach number 1.7 over a wedge of 25 degrees to the incident shock. Figure 15 shows the experimental results, kindly provided by Prof. K. Takayama, Shock Wave Research Center, Tohoku University, Japan. Figure 16 shows 100 contours of density computed by the WAF method and the present HLLC-Riemann solver. Figure 17 shows the corresponding computations using the exact Riemann solver. A grid of 350 by 200 was used in the computations. In this problem, in addition to the reflected shock and the Mach stem there is a contact surface emanating from the triple point. Note that the resolution of this feature with the present HLLC solver is virtually identical to that of the exact Riemann solver.

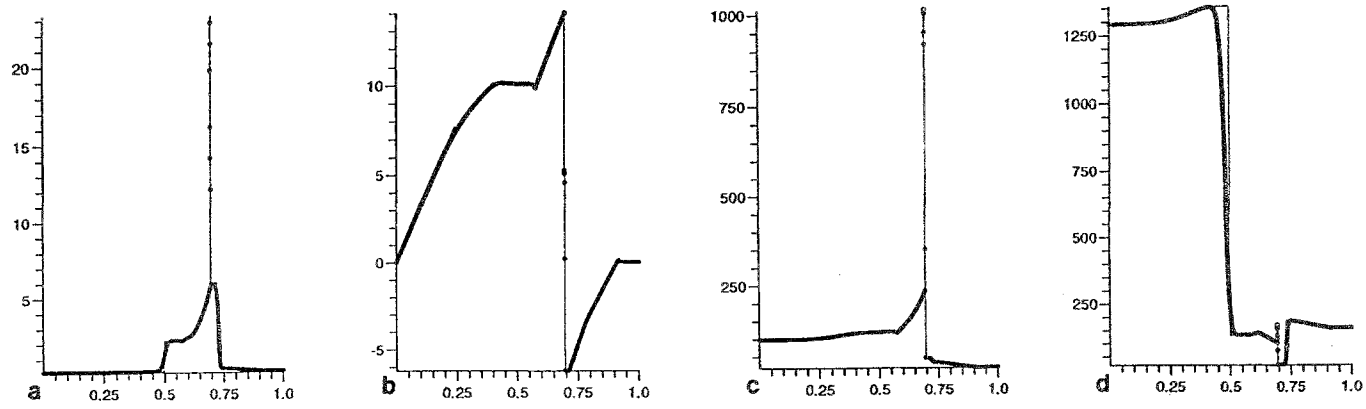

Fig. 12a–d. Comparison of performance between the original HLL (symbol) and the present HLLC (line) Riemann solvers used in the WAF method for the Woodward and Colella test problem at time 0.028 units: **a** density; **b** velocity; **c** pressure; **d** specific internal energy

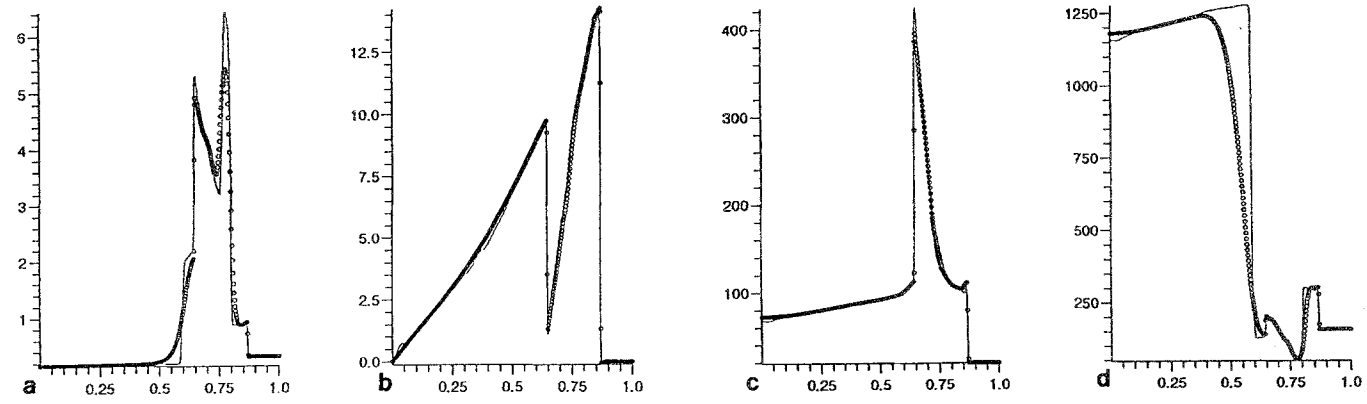

Fig. 13a–d. Comparison of performance between the original HLL (symbol) and the present HLLC (line) Riemann solvers used in the WAF method for the Woodward and Colella test problem at time 0.038 units: **a** density; **b** velocity; **c** pressure; **d** specific internal energy

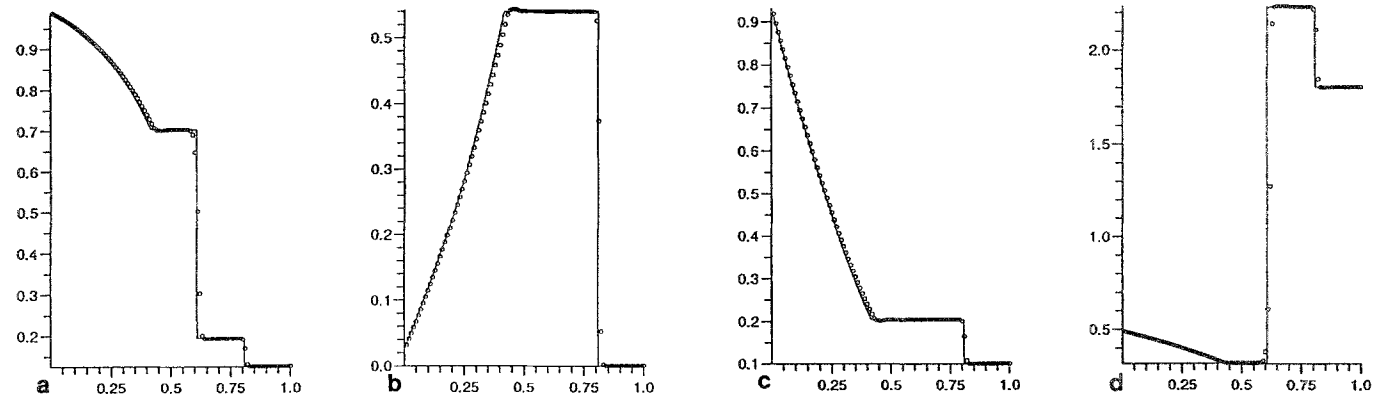

Fig. 14a–d. Comparison between the numerical (symbol) and exact solutions for Sod's problem with covolume at time 0.20 units: **a** density; **b** velocity; **c** pressure; **d** specific internal energy. Numerical method used is WAF with the present HLLC-Riemann solver

7. Conclusions

The missing contact discontinuity in the Harten-Lax-van Leer Riemann solver has been restored. Also, we have presented new ways of providing wave speed estimates. The resulting HLLC solver has then been implemented in the second-order WAF method. Numerical results for ideal gases in one and two dimensions and for covolume gases in one dimension have been presented. The numerical solutions obtained using the improved HLLC solver are comparable to those obtained using the exact Riemann solver and far superior to those obtained using the original HLL solver. For the simple equations of state considered the computing savings, relative to the exact solver, are modest (about 50 %). For more complex equations of state we expect these savings to be much more significant. In any case, the HLLC

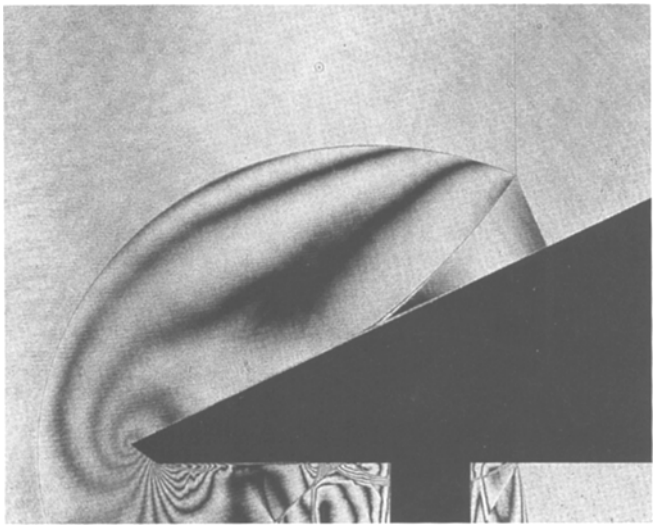

Fig. 15. Holographic interferogram of Mach reflection of an incident shock of Mach number 1.7 over a wedge at 25 degrees. Courtesy of Prof. K. Takayama, Shock Wave Research Center, Tohoku University, Japan

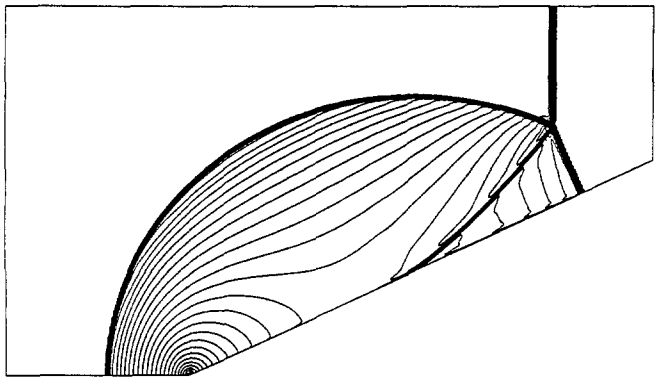

Fig. 16. Computed isopycnics of Mach reflection problem using the WAF method and the HLLC-Riemann solver. Compare with Figs. 15 and 17

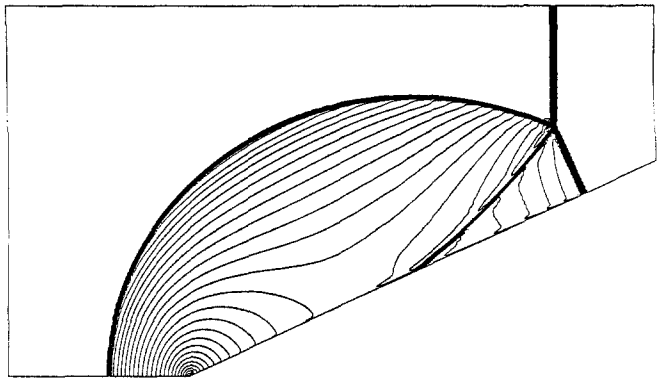

Fig. 17. Computed isopycnics of Mach reflection problem using the WAF method and the exact Riemann solver. Compare with Figs. 15 and 16

solver has two valuable additional advantages over the exact Riemann solver, namely simplicity and correct handling of sonic flow.

Acknowledgement. The computations of Figs. 16 and 17 were performed on the CRAY YMP 8 CPU of the Institute of Fluid Science, Tohoku University, Japan, while the first named author was a visiting Professor. The support provided is gratefully acknowledged.

References

Davis SF (1988) Simplified second-order Godunov-type methods. SIAM J Sci and Stat Comput 9:445

Einfeldt B (1988) On Godunov-type methods for the Euler equations with general equation of state. In: Proc Second Internat Conference on Hyperbolic Problems, Aachen, Germany.

Godunov SK (1959) A finite difference method for the numerical computation of discontinuous solutions of the equations of fluid dynamics. Mat Sb 47:357

Harten A, Lax PD, van Leer B (1983) On upstream differencing and Godunov-type schemes for hyperbolic conservation laws. SIAM Review 25:35–61

Roe PL (1981) Approximate Riemann solvers, parameter vectors, and difference schemes. J Comput Physics 43:357

Toro EF (1989a) A fast Riemann solver with constant covolume applied to the random choice method. Int J Numer Methods in Fluids 9:1145

Toro EF (1989b) A weighted average flux method for hyperbolic conservation laws. Proc Royal Soc London A 423:401

Toro EF (1991) A linearized Riemann solver for the Euler equations of gas dynamics. Proc Roy Soc London A 434:683

Toro EF (1992a) Riemann problems and the WAF method for solving the two-dimensional shallow water equations. Phil Trans Royal Soc London A 338:43

Toro EF (1992b) The weighted average flux method applied to the Euler equations. Phil Trans Roy Soc London A 341:499

Woodward P, Colella PJ (1984) The numerical simulation of two-dimensional fluid flow with strong shocks. J Comput Phys 54:115

This article was processed using Springer-Verlag TEX Shock Waves macro package 1.0 and the AMS fonts, developed by the American Mathematical Society.